RAA 2019 Vol. **19** No. **7**, 92(8pp) doi: 10.1088/1674–4527/19/7/92

http://www.raa-journal.org *http://iopscience.iop.org/raa*

***R**esearch in*
***A**stronomy and*
***A**strophysics*

The distance measurements of supernova remnants in the fourth Galactic quadrant

Su-Su Shan[1,2], Hui Zhu[1,3], Wen-Wu Tian[1,2], Hai-Yan Zhang[1], Ai-Yuan Yang[4] and Meng-Fei Zhang[1,2]

[1] Key Laboratory of Optical Astronomy, National Astronomical Observatories, Chinese Academy of Sciences, Beijing 100101, China; *shansusu@nao.cas.cn, zhuhui@nao.cas.cn*

[2] School of Astronomy, University of Chinese Academy of Sciences, Beijing 100049, China

[3] Harvard-Smithsonian Center for Astrophysics, 60 Garden Street, Cambridge, MA 02138, USA

[4] Max-Planck-Institut für Radioastronomie, Aufdem Hügel 60, D-53121, Bonn, Germany

Received 2018 November 25; accepted 2019 January 3

Abstract We take advantage of red clump stars to build the relation of the optical extinction (A_V) and distance in each direction of supernova remnants (SNRs) with known extinction in the fourth Galactic quadrant. The distances of nine SNRs are determined well by this method. Their uncertainties range from 10% to 30%, which are significantly improved for eight SNRs, G279.0+1.1, G284.3–1.8, G296.1–0.5, G299.2–2.9, G308.4–1.4, G309.2–0.6, G309.8–2.6 and G332.4–0.4. In addition, SNR G284.3–1.8 with the new distance of 5.5 kpc is not likely associated with the PSR J1016–5857 at 3 kpc.

Key words: ISM: supernova remnants — ISM: dust, extinction — stars: distances

1 INTRODUCTION

Distance is a basic and important parameter for a supernova remnant (SNR) to constrain its size, age, expansion velocity and explosion energy of the progenitor supernova (e.g., Tian & Leahy 2008; Zhou et al. 2018). However, it is challenging to obtain reliable distances of SNRs. About 30% of SNR distances are available in the Galactic SNR catalog of Green (2014) and $\sim$ 50% of SNRs have distances in the catalog of Ferrand & Safi-Harb (2012). Uncertainty estimates are not given for most of these distances.

There are several methods to measure the distance of SNRs. Firstly, the kinematic distances of SNRs are likely to be measured based on their HI absorptions or molecular line emissions from the clouds interacting with them (e.g., Leahy & Tian 2010; Su et al. 2011; Ranasinghe & Leahy 2018). Secondly, for shell-type radio SNRs, distances can be estimated by the $\Sigma - D$ relation (e.g., Case & Bhattacharya 1998). Thirdly, the distances of SNRs are usually equivalent to the distances of their possible associations, for example, OB associations (e.g. Cha et al. 1999, Vela remnant) and pulsars (e.g. Cordes & Lazio 2002). For some rare SNRs, distances can also be obtained by proper motion (e.g. Vink 2008; Katsuda et al. 2008, Kepler's SNR), Sedov estimates (Bocchino et al. 2000), blast wave method (McKee & Cowie 1975) or extinction measurement (Chen et al. 2017; Zhao et al. 2018).

Red clump (RC) stars are characterized by their concentration in an obvious region of the color-magnitude diagram (CMD) (Gao et al. 2009). They are usually low mass stars in the early stage of core-He burning and are widely used to trace distances, and probe extinction towards Galactic objects since the dispersions of their absolute magnitude and intrinsic color are small (Girardi 2016). The relation of extinction and distance has been used to estimate the distances of these objects in cases with known extinction, such as pulsars (Durant & van Kerkwijk 2006) and low-mass X-ray binaries (Güver et al. 2010). Zhu et al. (2015) first applied the RC method to determine the distance of SNR G332.5–5.6. Shan et al. (2018) applied a similar method to systematically analyze the extinction distances towards SNRs in the first Galactic quadrant and independently obtained new extinction distances of 15 SNRs. Their results have demonstrated that the distances traced by RC stars are reliable and consistent with kinematic distances. This paper presents our new results aiming at the SNRs in the other Galactic quadrants.

2 METHOD

We follow the RC method of Shan et al. (2018). Here we briefly describe this method. To select RC stars, we build the Ks (hereafter K) vs. $J-K$ CMD in the direction of each SNR with the 2MASS All-Sky Point Source Catalog (Skrutskie et al. 2006). The area around the SNR is $1^\circ \times 0.5^\circ$ ($\Delta l \times \Delta b$). Figure 1(a) displays an example for SNR 308.2–1.4.

We bin the star sample into a number of horizontal strips according to K magnitude. The sample for each bin is constructed as the star count histogram. Then we use the function below to fit the histogram (Durant & van Kerkwijk 2006)

$$N = A_{\rm RCs} \exp\left\{\frac{-[(J-K)-(J-K)_{\rm peak}]^2}{2\sigma^2}\right\} + A_C(J-K)^\alpha \ . \quad (1)$$

Here $(J-K)$ represents the stellar color, and $A_{\rm RCs}$ and A_C stand for the normalizations of RC stars and contaminant stars, respectively. The first term is a Gaussian function to fit the RC star distribution; the second term is a power law to fit the contaminant stars (see Fig. 1(b)). The best fit yields the stellar color of RC stars at peak density $(J-K)_{\rm peak}$ for each strip. The extinction and distance are calculated from

$$A_K = 0.67 \times [(J-K)_{\rm peak} - (J-K)_0] \ , \quad (2)$$

$$\frac{A_K}{A_V} = 0.1615 - \frac{0.1483}{R_V} \ , \quad (3)$$

$$D({\rm kpc}) = 10^{[0.2(m_K - M_K + 5 - 0.1137 A_V)]}/1000 \ . \quad (4)$$

Here A_V and A_K are extinction in the V and K bands respectively. We adopt the total to selective extinction ratio $R_V = 3.1 \pm 0.18$ (Schlafly et al. 2016), the intrinsic color of RC stars $(J-K)_0 = 0.63 \pm 0.1$ mag (e.g., Yaz Gökçe et al. 2013; Grocholski & Sarajedini 2002) and the absolute magnitude of RC stars $M_K = -1.61 \pm 0.1$ mag (e.g., Alves 2000; Grocholski & Sarajedini 2002; Hawkins et al. 2017). The uncertainties of R_V, $(J-K)_0$ and M_K are transferred to A_V and D via an error propagation formula (see Shan et al. (2018) and references therein).

In Figure 1(c), the relation between the optical extinction A_V and distance D (hereafter, $A_V - D$) is built along the direction of G308.4–1.4. Combining the A_V value of G308.4–1.4, its distance is estimated by the Bayesian method (Güver et al. 2010). Figure 1(d) shows the probability distribution over distance calculated by

$$P(D) = \int P_{\rm SNR}(A_K) P_{\rm RC}(D|A_V) dA_V \ . \quad (5)$$

Here $P_{\rm SNR}(A_V)$ represents the probability distribution for an SNR's extinction. We assume $P_{\rm RC}(D|A_V) = P_{\rm RC}(A_V|D)$. $P_{\rm RC}(A_V|D)$ signifies the distribution of the extinction traced by the RC at each distance bin. Both distributions are assumed to be Gaussian functions. Then we fit these distributions by a Gaussian function, yielding the distance with the highest probability. For the objects with good Gaussian fitting, the uncertainty in distance is equal to the standard deviation of the Gaussian. However, for some objects, there are apparent and sudden decreases in the distance probability. The red lines mark such decreases (see Fig. 3). In this case, the uncertainty in distance reflects the cut-off distance.

3 RESULTS AND BRIEF DISCUSSION

New distances for nine SNRs are obtained. The results are summarized in Tables 1 and 2. We also note that this method does not work for SNRs in the second and third quadrants after tens of trials. This might be caused by the fact that the extinction towards our targets in the two quadrants grows slowly with increasing distance, which makes the $A_V - D$ relation too flat to give a reliable distance. Hence, we just discuss the results from the fourth quadrant. Figure 2 presents the CMDs with the locations of the RC's peak density in the direction of SNRs. Figure 3 shows the corresponding $A_V - D$ relations and probability distribution over distance for each SNR and the best-fit Gaussian model. We discuss them in detail below.

G279.0+1.1

The distance of G279.0+1.1 is estimated at 3 kpc by the blast wave method and $\Sigma - D$ relation (McKee & Cowie 1975; Stupar & Parker 2009). However, Stupar & Parker (2009) warned that this distance should be treated with caution since McKee & Cowie (1975)'s estimate depends on the initial explosion energy of the progenitor star and the $\Sigma - D$ relation might have an error up to 40%. Our RC method estimates its distance as 2.7 ± 0.3 kpc which coincides with the previous measurements.

G284.3–1.8

G284.3–1.8 was suggested to be associated with the pulsar PSR J1016-5857 (3 kpc, (Kargaltsev et al. 2013)) or the γ-ray binary 1FGL J1018.6–5856 ($5.6^{+4.6}_{-2.1}$ kpc (Napoli et al. 2011)). We estimate its distance at 5.5 ± 0.7 kpc. The new distance indicates that G284.3–1.8 is not likely to be associated with PSR J1016-5857 at 3 kpc.

G296.1–0.5

G296.1–0.5 is a middle-aged SNR with complex structures. Longmore et al. (1977) estimated its distance between 3 and 5 kpc from two independent ways of red-

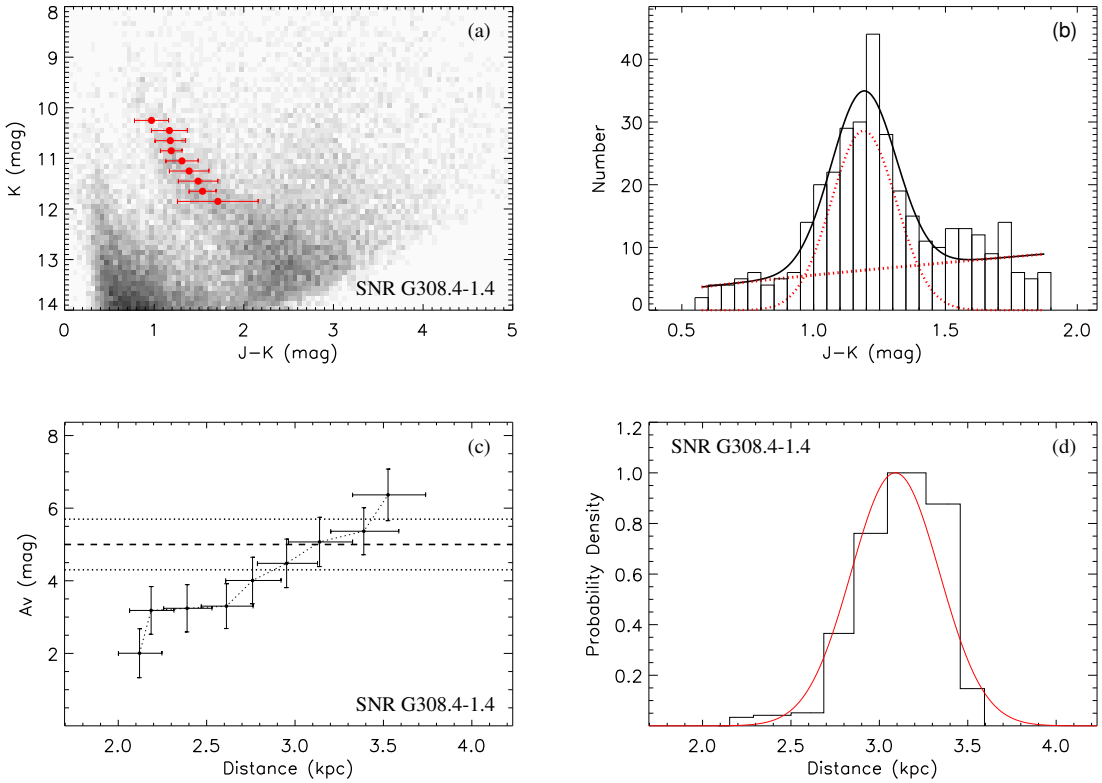

Fig. 1 (a) The CMD in the direction of G308.4–1.4 within 0.5 deg^2. The *red dots* and *red lines* mark the fitted locations of the RC peak density and its extent with 1σ. (b) Histogram of the $J-K$ values for the selected stars in $10.6 < K < 11.1$. The *black curve* is the best fit to this histogram. The *red dotted curves* are the Gaussian and power-law components. (c) The $A_V - D$ relation in the direction of G308.4–1.4. The *dashed line* is the A_V value of this SNR. The *dotted lines* are the uncertainties of A_V. (d) Probability distribution over distance to the SNRs and the best-fit Gaussian model (*Color version of Figs. 1–4 is online*).

Table 1 Optical Extinction A_V and Distance

Source name	A_V (mag)	Distance (kpc)	Previous measurement (kpc)	Method	Reference
G279.0+1.1	1.6±0.1	2.7±0.3	3	Blast wave and $\Sigma - D$	[1]
G284.3–1.8	4.4[1]	5.5±0.7	3, $5.6^{+4.6}_{-2.1}$	Distance of association	[2], [3], [4]
G296.1–0.5	1.9±0.3	4.3±0.8	3±1.0	Reddening measurement	[5], [6]
			3.8±1.9	Kinematic measurement	[5], [6]
			7.7, 6.6, 4.9	$\Sigma - D$	[7], [8], [9]
G315.4–2.3	1.7±0.2	≤ 2.0	2.8±0.4, 2.3±0.2	Kinematic measurement	[10], [11], [12]
			1.2 ± 0.2	Sedov estimate	[13]
G332.4–0.4	4.7±0.7	3.0±0.3	3.3, 3.1-4.6	Kinematic measurement	[14], [10], [15]
			6.5	Extinction measurement	[16]

Notes: [1] We assume the error of A_V as 10% when determining the distance of G284.3–1.8. References: [1] Stupar & Parker (2009); [2] H. E. S. S. Collaboration et al. (2012); [3] Kargaltsev et al. (2013); (4) Napoli et al. (2011); [5] Castro et al. (2011); [6] Longmore et al. (1977); [7] Caswell & Barnes (1983); [8] Case & Bhattacharya (1998); [9] Clark et al. (1973); [10] Zhu et al. (2017); [11] Rosado et al. (1996); [12] Sollerman et al. (2003); [13] Bocchino et al. (2000); [14] Caswell et al. (1975); [15] Reynoso et al. (2004); [16] Ruiz (1983).

dening measurements and kinematic method. Distances calculated by the $\Sigma - D$ relation are 7.7, 6.6 and 4.9 kpc from Caswell & Barnes (1983), Case & Bhattacharya (1998) and Clark et al. (1973), respectively. We find its distance to be 4.3±0.8 kpc, which further supports the results of Longmore et al. (1977) and Clark et al. (1973).

G315.4–2.3 (RCW 86)

Rosado et al. (1996) fitted the radial velocity of H_α with respect to the local standard of rest and converted it to

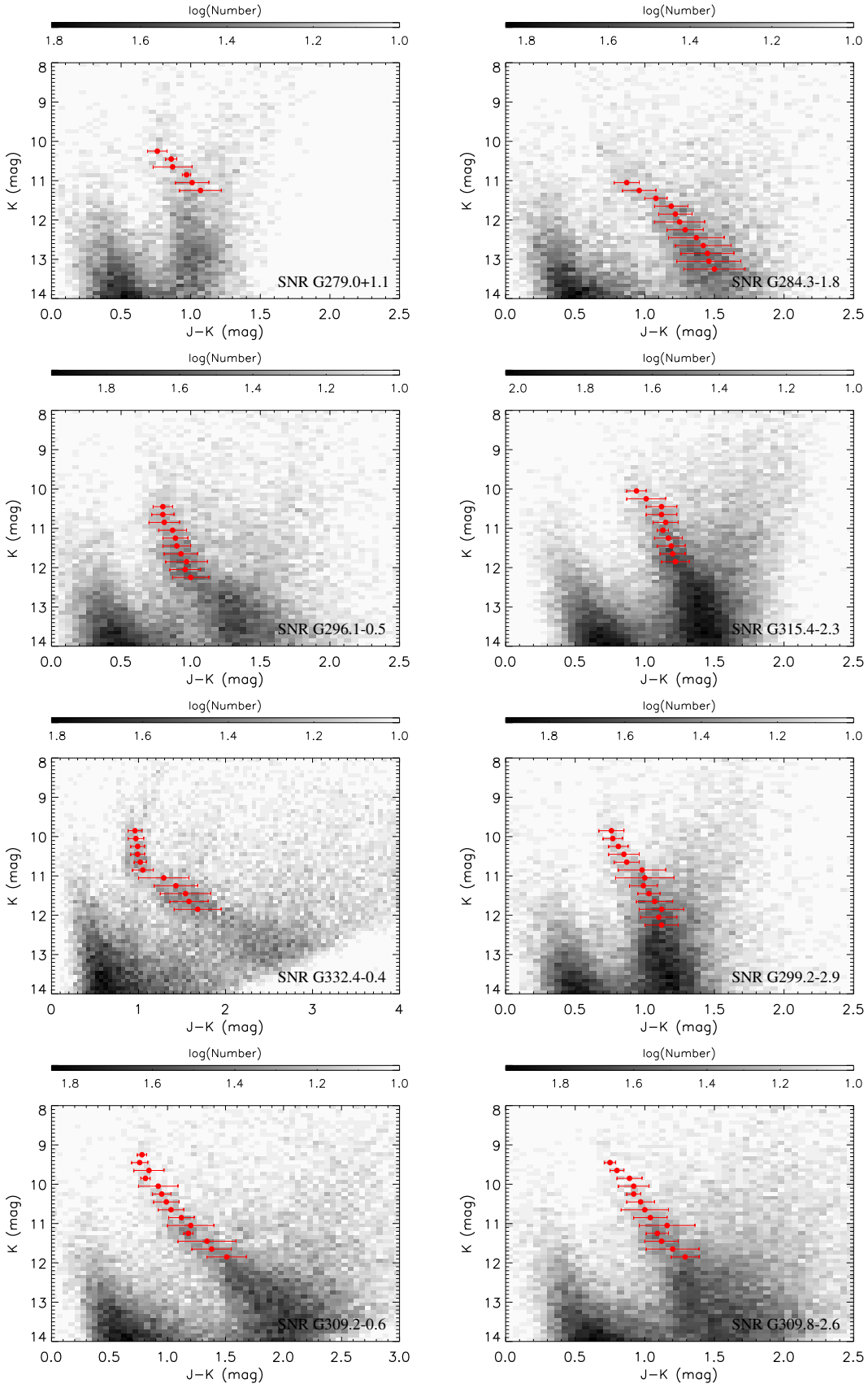

Fig. 2 The CMDs within 0.5 deg^2 in the directions of eight SNRs. The grey colors denote stellar densities in the logarithmic scale. The *red dots* and *lines* mark the fitted location of the RC peak density and its extent with 1σ respectively.

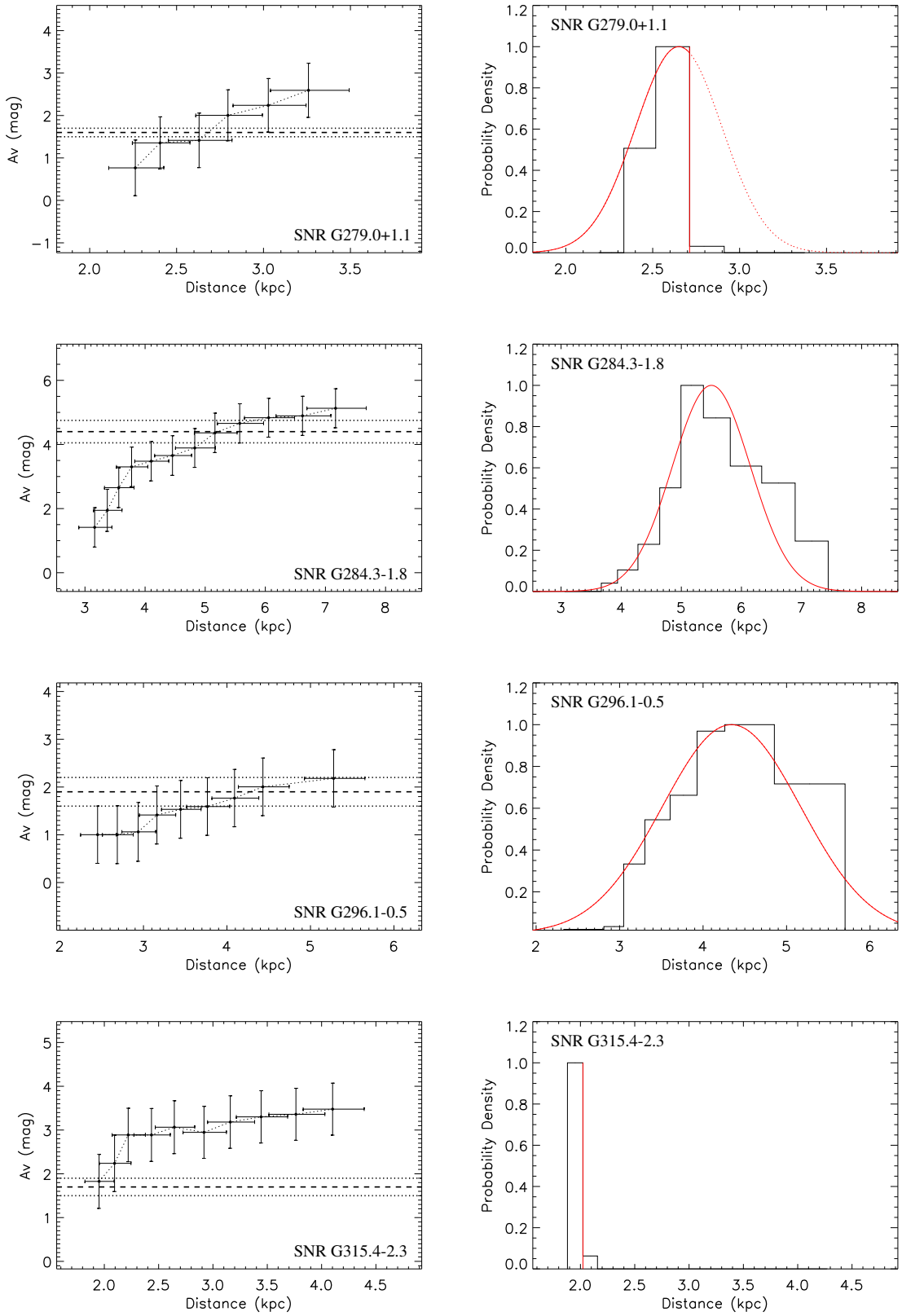

Fig. 3 *Left*: The $A_V - D$ relation traced by RC stars along the direction of each SNR. The *dashed line* is the A_V value of each SNR. The *dotted lines* are the uncertainties of A_V. *Right*: Probability distribution over distance to the SNRs and the best-fit Gaussian model with the cutoffs. The *red line* in the right panel for G315.4–2.3 is the upper limit of distance.

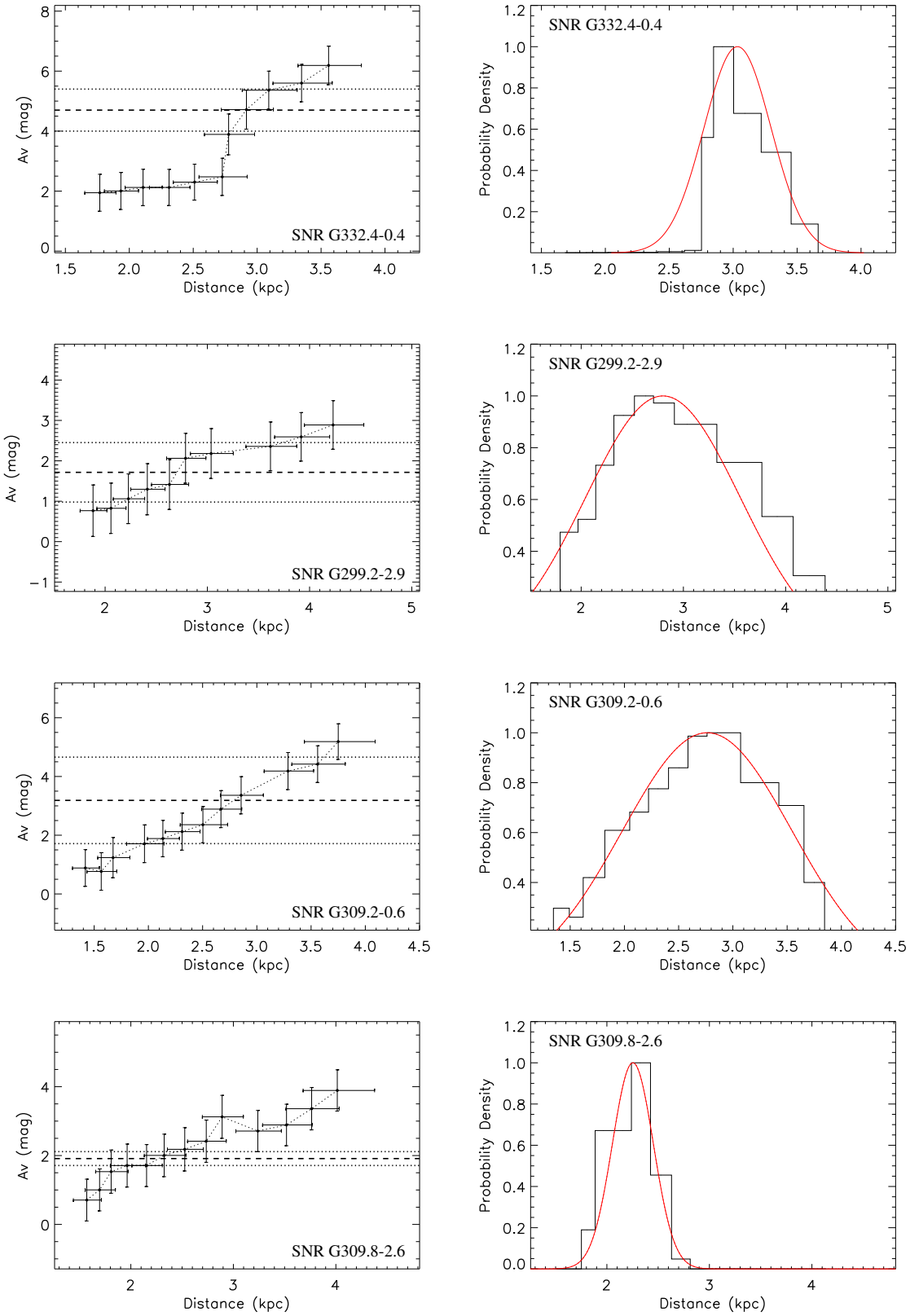

Fig. 3 — *Continued.*

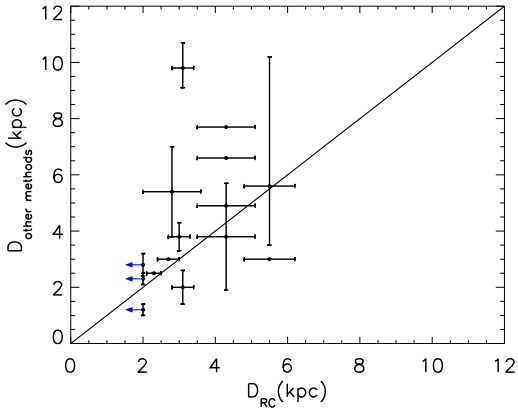

Fig. 4 Comparison of the RC distances and the distances determined by other methods. The *blue arrows* represent the upper limits of distances for G315.4–2.3. The data are based on Tables 1 and 2.

Table 2 A_V Converted from Hydrogen Column Density $N_{\rm H}$ and Distance

Source Name	$N_{\rm H}$ (10^{21} cm^{-2})	A_V^1 (mag)	Distance (kpc)	Previous measurement (kpc)	Method	Reference
G299.2–2.9	3.5±1.5	1.7±0.7	2.8±0.8	0.5, 2–11	Hydrogen column density	[1], [2]
G308.4–1.4	10.2±1.4	5±0.7	3.1±0.3	5.9±2.0	Extinction estimate	[3]
				2.0 ± 0.6, 12.5±0.7	Kinematic measurement	[3]
				$9.8^{+0.9}_{-0.7}$	Sedov estimate	[3]
G309.2–0.6	6.5±3.0	3.2±1.5	2.8±0.8	4 ± 2	Hydrogen column density	[4]
				5.4±1.6 to 14.1±0.7	Kinematic measurement	[5]
G309.8–2.6	3.9±0.4	1.9±0.2	2.3±0.2	2.5	Pulsar distance	[6], [7]

Notes: [1] $A_V = N_{\rm H}/(2.04\pm0.05)\times10^{21}$ cm^{-2} mag^{-1} (Zhu et al. 2017). References: [1] Park et al. (2007); [2] Slane et al. (1996); [3] Prinz & Becker (2012); [4] Rakowski et al. (2001); [5] Gaensler et al. (1998); [6] Lemoine-Goumard et al. (2011); [7] Camilo et al. (2004).

a kinematic distance of 2.8±0.4 kpc for G315.4–2.3 based on the Galactic rotation curve. Sollerman et al. (2003) followed this method with high resolution spectroscopic data and constrained the distance as 2.3±0.2 kpc. These distances were supported by the combination of proper motion and post-shock temperature (Helder et al. 2013). A smaller distance of $1.2^{+0.2}_{-0.2}$ kpc was determined with Sedov estimates (Bocchino et al. 2000). There is a cutoff in the probability distribution of distance because only the upper limit for A_V of G315.4–2.3 is in the range of A_V traced by the RC stars. Therefore, the red line in the right panel for G315.4–2.3 is the upper limit of distance, estimated to be 2.0 kpc by the RC method.

G332.4–0.4 (RCW 103)

The kinematic distance based on HI absorption spectrum is about 3.3 kpc for RCW 103 (Caswell et al. 1975; Reynoso et al. 2004). Ruiz (1983) estimated its distance to be around 6.5 kpc by extinction measurement. However, the extinction traced by RC stars infers that this SNR is located at 3.0±0.3 kpc, which is consistent with the kinematic distance.

G299.2–2.9

We derive an RC distance of G299.2–2.9 at 2.8±0.8 kpc for the first time. A low interstellar column density in the line of sight hinted at a very nearby distance (∼0.5 kpc) based on the *ROSAT* Position Sensitive Proportional Counter observation (Slane et al. 1996). However, spatially resolved spectroscopy with the *Chandra X-Ray Observatory* indicated a higher hydrogen column density ($N_{\rm H} \sim 3.5\times10^{21}$ cm^{-2}), which suggested a distance of 2–11 kpc (Park et al. 2007). The RC distance is the best so far.

G308.4–1.4

Prinz & Becker (2012) published a detailed analysis of the distance to G308.4–1.4: (1) the distance indicated by extinction is 5.9±2.0 pc; (2) a kinematic distance is 2.0 ± 0.6 kpc or 12.5±0.7 kpc; (3) the Sedov-analysis-based distance is $9.8^{+0.9}_{-0.7}$ kpc. The RC distance of this SNR is 3.1±0.3 kpc, which is consistent with the lower limits of extinction distance and kinematic distance.

G309.2–0.6

HI absorption against G309.2–0.6 yielded a kinematic distance from 5.4±1.6 to 14.1±0.7 kpc (Gaensler et al. 1998). Rakowski et al. (2001) estimated the distance of

this SNR to be 4 ± 2 kpc from the foreground hydrogen column density. The distance measured by the RC method is 2.8 ± 0.8 kpc, which is consistent with the lower limits of previous measurements.

G309.8–2.6

We estimate the distance of G309.8–2.6 at 2.3 ± 0.2 kpc for the first time. The RC distance further supports that G309.8–2.6 is associated with the very young pulsar PSR J1357–6429 located at 2.5 kpc (Camilo et al. 2004).

We compare the nine RC distances of SNRs with the distances from other methods in Figure 4. Note that there might be several distance measurements for one SNR and a few of them do not have uncertainty estimates. The RC distances are generally consistent with the previous measurements within error bars. The distance uncertainties from the RC method range from 10% to 30% and the accuracies of distances are significantly improved for eight SNRs.

Acknowledgements We all acknowledge supports from the National Key R&D Programs of China (2018YFA0404203) and the National Natural Science Foundation of China (Grant Nos. 11603039 and U1831128). We highly appreciate the anonymous referee for helpful comments.

References

Alves, D. R. 2000, ApJ, 539, 732
Bocchino, F., Vink, J., Favata, F., Maggio, A., & Sciortino, S. 2000, A&A, 360, 671
Camilo, F., Manchester, R. N., Lyne, A. G., et al. 2004, ApJ, 611, L25
Case, G. L., & Bhattacharya, D. 1998, ApJ, 504, 761
Castro, D., Slane, P. O., Gaensler, B. M., Hughes, J. P., & Patnaude, D. J. 2011, ApJ, 734, 86
Caswell, J. L., & Barnes, P. L. 1983, ApJ, 271, L55
Caswell, J. L., Murray, J. D., Roger, R. S., Cole, D. J., & Cooke, D. J. 1975, A&A, 45, 239
Cha, A. N., Sembach, K. R., & Danks, A. C. 1999, ApJ, 515, L25
Chen, B.-Q., Liu, X.-W., Ren, J.-J., et al. 2017, MNRAS, 472, 3924
Clark, D. H., Caswell, J. L., & Green, A. J. 1973, Nature, 246, 28
Cordes, J. M., & Lazio, T. J. W. 2002, astro-ph/0207156
Durant, M., & van Kerkwijk, M. H. 2006, ApJ, 650, 1070
Ferrand, G., & Safi-Harb, S. 2012, Advances in Space Research, 49, 1313
Gaensler, B. M., Green, A. J., & Manchester, R. N. 1998, MNRAS, 299, 812
Gao, J., Jiang, B. W., & Li, A. 2009, ApJ, 707, 89
Girardi, L. 2016, ARA&A, 54, 95
Green, D. A. 2014, Bulletin of the Astronomical Society of India, 42, 47
Grocholski, A. J., & Sarajedini, A. 2002, AJ, 123, 1603
Güver, T., Özel, F., Cabrera-Lavers, A., & Wroblewski, P. 2010, ApJ, 712, 964
H. E. S. S. Collaboration, Abramowski, A., Acero, F., et al. 2012, A&A, 541, A5
Hawkins, K., Leistedt, B., Bovy, J., & Hogg, D. W. 2017, MNRAS, 471, 722
Helder, E. A., Vink, J., Bamba, A., et al. 2013, MNRAS, 435, 910
Kargaltsev, O., Rangelov, B., & Pavlov, G. G. 2013, arXiv:1305.2552
Katsuda, S., Tsunemi, H., Uchida, H., & Kimura, M. 2008, ApJ, 689, 225
Leahy, D., & Tian, W. 2010, in Astronomical Society of the Pacific Conference Series, 438, The Dynamic Interstellar Medium: A Celebration of the Canadian Galactic Plane Survey, eds. R. Kothes, T. L. Landecker, & A. G. Willis, 365
Lemoine-Goumard, M., Zavlin, V. E., Grondin, M.-H., et al. 2011, A&A, 533, A102
Longmore, A. J., Clark, D. H., & Murdin, P. 1977, MNRAS, 181, 541
McKee, C. F., & Cowie, L. L. 1975, ApJ, 195, 715
Napoli, V. J., McSwain, M. V., Marsh Boyer, A. N., & Roettenbacher, R. M. 2011, PASP, 123, 1262
Park, S., Slane, P. O., Hughes, J. P., et al. 2007, ApJ, 665, 1173
Prinz, T., & Becker, W. 2012, A&A, 544, A7
Rakowski, C. E., Hughes, J. P., & Slane, P. 2001, ApJ, 548, 258
Ranasinghe, S., & Leahy, D. A. 2018, AJ, 155, 204
Reynoso, E. M., Green, A. J., Johnston, S., et al. 2004, PASA, 21, 82
Rosado, M., Ambrocio-Cruz, P., Le Coarer, E., & Marcelin, M. 1996, A&A, 315, 243
Ruiz, M. T. 1983, AJ, 88, 1210
Schlafly, E. F., Meisner, A. M., Stutz, A. M., et al. 2016, ApJ, 821, 78
Shan, S. S., Zhu, H., Tian, W. W., et al. 2018, ApJS, 238, 35
Skrutskie, M. F., Cutri, R. M., Stiening, R., et al. 2006, AJ, 131, 1163
Slane, P., Vancura, O., & Hughes, J. P. 1996, ApJ, 465, 840
Sollerman, J., Ghavamian, P., Lundqvist, P., & Smith, R. C. 2003, A&A, 407, 249
Stupar, M., & Parker, Q. A. 2009, MNRAS, 394, 1791
Su, Y., Chen, Y., Yang, J., et al. 2011, ApJ, 727, 43
Tian, W. W., & Leahy, D. A. 2008, MNRAS, 391, L54
Vink, J. 2008, ApJ, 689, 231
Yaz Gökçe, E., Bilir, S., Öztürkmen, N. D., et al. 2013, New Astron., 25, 19
Zhao, H., Jiang, B., Gao, S., Li, J., & Sun, M. 2018, ApJ, 855, 12
Zhou, P., Vink, J., Li, G., & Domček, V. 2018, ApJ, 865, L6
Zhu, H., Tian, W., Li, A., & Zhang, M. 2017, MNRAS, 471, 3494
Zhu, H., Tian, W. W., & Wu, D. 2015, MNRAS, 452, 3470